Vortex algebra by multiply cascaded four-wave mixing of femtosecond optical beams

Peter Hansinger[1,*], Georgi Maleshkov[2], Ivan L. Garanovich[3], Dmitry V. Skryabin[4], Dragomir N. Neshev[3], Alexander Dreischuh[2] and Gerhard G. Paulus[1,5]

[1] *Institute for Optics and Quantum Electronics, Friedrich-Schiller-University, Max-Wien-Platz 1, D-07743 Jena, Germany*

peter.hansinger@uni-jena.de

[2] *Department of Quantum Electronics, Sofia University, 5, J. Bourchier Blvd., Sofia-1164, Bulgaria*

[3] *Nonlinear Physics Centre, Research School of Physics and Engineering, Australian National University, Canberra, Australia*

[4] *University of Bath, Bath, United Kingdom*

[5] *Helmholtz Institute Jena, Helmholtzweg 4, D-07743 Jena, Germany*

Abstract: Experiments performed with different vortex pump beams show for the first time the algebra of the vortex topological charge cascade, that evolves in the process of nonlinear wave mixing of optical vortex beams in Kerr media due to competition of four-wave mixing with self- and cross-phase modulation. This leads to the coherent generation of complex singular beams within a spectral bandwidth larger than 200nm. Our experimental results are in good agreement with frequency-domain numerical calculations that describe the newly generated spectral satellites.

OCIS codes: (190.0190) Nonlinear optics, (190.4380) Nonlinear optics, four-wave mixing.

References and links

1. E. H. Brandt, J. Vanacken, and V. V. Moshchalkov, "Vortices in physics," Physica C: Superconductivity **369**, 1–9 (2002).
2. M. R. Dennis, R. P. King, B. Jack, K. O'Holleran, and M. J. Padgett, "Isolated optical vortex knots," Nature Physics **6**, 118–121 (2010).
3. M. R. Matthews, B. P. Anderson, P. C. Haljan, D. S. Hall, C. E. Wieman, and E. A. Cornell, "Vortices in a Bose-Einstein condensate," Physical Review Letters **83**, 2498–2501 (1999).
4. J. L. Thomas and R. Marchiano, "Pseudo angular momentum and topological charge conservation for nonlinear acoustical vortices," Physical Review Letters **91**, 244302 (2003).
5. T. Brunet, J. L. Thomas, R. Marchiano, and F. Coulouvrat, "Experimental observation of azimuthal shock waves on nonlinear acoustical vortices," New Journal of Physics **11**, 13002 (2009).
6. Y. Ueno, Y. Toda, S. Adachi, R. Morita, and T. Tawara, "Coherent transfer of orbital angular momentum to excitons by optical four-wave mixing," Optics Express **17**, 20567–20574 (2009).
7. S. L. Rolston and W. D. Phillips, "Nonlinear and quantum atom optics," Nature **416**, 219–224 (2002).
8. T. P. Simula, N. Nygaard, S. X. Hu, L. A. Collins, B. I. Schneider, and K. Molmer, "Angular momentum exchange between coherent light and matter fields," Physical Review A **77**, 15401 (2008).
9. L. Deng, E. W. Hagley, J. Wen, M. Trippenbach, Y. Band, P. S. Julienne, J. E. Simsarian, K. Helmerson, S. L. Rolston, and W. D. Phillips, "Four-wave mixing with matter waves," Nature **398**, 218–220 (1999).

10. J. E. Williams and M. J. Holland, "Preparing topological states of a Bose-Einstein condensate," Nature **401**, 568–572 (1999).
11. K. W. Madison, F. Chevy, W. Wohlleben, and J. Dalibard, "Vortex formation in a stirred Bose-Einstein condensate," Physical Review Letters **84**, 806–809 (2000).
12. M. F. Andersen, C. Ryu, P. Clade, V. Natarajan, A. Vaziri, K. Helmerson, and W. D. Phillips, "Quantized rotation of atoms from photons with orbital angular momentum," Physical Review Letters **97**, 170406 (2006).
13. J. F. Nye and M. V. Berry, "Dislocations in wave trains," Proceedings of the Royal Society of London. A. Mathematical and Physical Sciences **336**, 165 (1974).
14. A. S. Desyatnikov, Y. S. Kivshar, and L. Torner, "Optical vortices and vortex solitons," Progress in Optics **47**, 291–391 (2005).
15. H. He, M. E. J. Friese, N. R. Heckenberg, and H. Rubinsztein-Dunlop, "Direct observation of transfer of angular momentum to absorptive particles from a laser beam with a phase singularity," Physical Review Letters **75**, 826–829 (1995).
16. D. G. Grier, "A revolution in optical manipulation," Nature **424**, 810–6 (2003).
17. G. Foo, D. M. Palacios, and G. A. Swartzlander Jr, "Optical vortex coronagraph." Optics Letters **30**, 3308–10 (2005).
18. G. Molina-Terriza, J. P. Torres, and L. Torner, "Twisted photons," Nature Physics **3**, 305–310 (2007).
19. W. J. Firth and D. V. Skryabin, "Optical Solitons Carrying Orbital Angular Momentum," Physical Review Letters **79**, 2450–2453 (1997).
20. K. Dholakia, N. B. Simpson, M. J. Padgett, and L. Allen, "Second-harmonic generation and the orbital angular momentum of light," Physical Review A **54**, 3742–3745 (1996).
21. J. Arlt, K. Dholakia, L. Allen, and M. J. Padgett, "Parametric down-conversion for light beams possessing orbital angular momentum," Physical Review A **59**, 3950 (1999).
22. S. Sogomonian, U. T. Schwarz, and M. Maier, "Phase-front transformation of a first-order Bessel beam in Raman-resonant four-wave mixing," Journal of the Optical Society of America B **18**, 497–504 (2001).
23. K. Bezuhanov, A. Dreischuh, G. G. Paulus, M. G. Schatzel, and H. Walther, "Vortices in femtosecond laser fields," Optics Letters **29**, 1942–1944 (2004).
24. I. Zeylikovich, H. I. Sztul, V. Kartazaev, T. Le, and R. R. Alfano, "Ultrashort Laguerre-Gaussian pulses with angular and group velocity dispersion compensation," Optics Letters **32**, 2025–2027 (2007).
25. I. G. Mariyenko, J. Strohaber, and C. J. Uiterwaal, "Creation of optical vortices in femtosecond pulses," Optics Express **13**, 7599–7608 (2005).
26. G. A. Swartzlander Jr, "Achromatic optical vortex lens," Optics Letters **31**, 2042–2044 (2006).
27. A. Vinçotte and L. Bergé, "Femtosecond optical vortices in air," Physical Review Letters **95**, 193901 (2005).
28. L. T. Vuong, T. Grow, A. Ishaaya, A. L. Gaeta, G. W. 't Hooft, E. R. Eliel, and G. Fibich, "Collapse of Optical Vortices," Physical Review Letters **96**, 2–5 (2006).
29. A. V. Gorbach and D. V. Skryabin, "Cascaded generation of multiply charged optical vortices and spatiotemporal helical beams in a Raman medium," Physical Review Letters **98**, 243601 (2007).
30. J. Strohaber, M. Zhi, A. V. Sokolov, A. A. Kolomenskii, G. G. Paulus, and H. A. Schuessler, "Coherent transfer of optical orbital angular momentum in multi-order Raman sideband generation," Optics Letters **37**, 3411–3413 (2012).
31. W. Jiang, Q.-F. Chen, Y.-S. Zhang, and G.-C. Guo, "Computation of topological charges of optical vortices via nondegenerate four-wave mixing," Physical Review A **74**, 1–4 (2006).
32. Y. Zhang, Z. Nie, Y. Zhao, C. Li, R. Wang, J. Si, and M. Xiao, "Modulated vortex solitons of four-wave mixing," Optics Express **18**, 10963–72 (2010).
33. F. Lenzini, S. Residori, F. T. Arecchi, and U. Bortolozzo, "Optical vortex interaction and generation via nonlinear wave mixing," Physical Review A **84**, 61801 (2011).
34. D. N. Neshev, A. Dreischuh, G. Maleshkov, M. Samoc, and Y. S. Kivshar, "Supercontinuum generation with optical vortices," Optics Express **18**, 18368–18373 (2010).
35. P. Del'Haye, A. Schliesser, O. Arcizet, T. Wilken, R. Holzwarth, and T. J. Kippenberg, "Optical frequency comb generation from a monolithic microresonator," Nature **450**, 1214–1217 (2007).
36. V. Tikhonenko, J. Christou, and B. Luther-Daves, "Spiraling bright spatial solitons formed by the breakup of an optical vortex in a saturable self-focusing medium," Journal of the Optical Society of America B **12**, 2046 (1995).
37. H. Saito and M. Ueda, "Split instability of a vortex in an attractive Bose-Einstein condensate," Physical Review Letters **89**, 190402 (2002).
38. A. Börzsönyi and Z. Heiner, "Dispersion measurement of inert gases and gas mixtures at 800 nm," Applied Optics **47**, 4856–4863 (2008).
39. M. Quiroga-Teixeiro, "Stable azimuthal stationary state in quintic nonlinear optical media," Journal of the Optical Society of America B **14**, 2004–2009 (1997).

1. Introduction

As an intriguing phenomenon in nature, vortices have become an important topic in many fields of physics, spanning from fluid dynamics [1], optics [2] to Bose-Einstein condensates [3]. Extensive research on both linear and nonlinear singular waves has been performed, illustrating the universality of vortices in the physical domain: Topological charge conservation using the concept of pseudo angular momentum was demonstrated in the harmonic generation of acoustic vortices [4], leading to the formation of angular shock waves [5]. Transfer of angular momentum from light to excitons in GaN was demonstrated by Ueno et al. [6]. Particularly interesting is the analogy between optical vortices and their atomic counterparts, coherent vortex wave functions in Bose-Einstein condensates [7], especially because angular momentum can be transferred between both [8]. Due to the close analogy between the Gross-Pitaevskii equation that governs BEC dynamics and the Nonlinear Schroedinger equation of nonlinear optics, the results presented here are also applicable to BECs and superfluids: While four-wave mixing of wave functions in BECs [9] and the generation of vortices by means of different methods [3, 10, 11, 12] have been demonstrated, the combination of both has not yet been observed. In this paper we present results of the analogous process in optics, and show, for the first time, cascaded nonlinear angular momentum mixing and coherent transfer of phase singularities over multiple orders.

In the optical domain, vortices are identified as helical phase profiles within a light beam, with a characteristic dependence $exp(im\phi)$ on the transverse angular coordinate ϕ [13]. The central singular point of this helix possesses no defined phase and therefore the intensity must vanish, leading to a characteristic cusp-like vortex core [14]. Such beams carry photon angular momentum, which can also be transferred to matter [15]. The angular momentum is proportional to the topological charge (TC) m of the optical vortex, associated with the total phase change $m \cdot 2\pi$ after one revolution around the core. Optical vortex beams have found various useful applications, namely in optical tweezers [16], coronagraphs [17] or as potential information carriers in data processing [18]. Of particular interest are nonlinear processes involving vortex beams, where conservation of the total orbital momentum determines particle-like dynamics of the filaments resulting from the modulational instability (MI) induced vortex break-up [19]. Conservation of the total orbital momentum also plays a profound role in second harmonic generation [20], parametric down-conversion [21] and stimulated Raman scattering [22] involving optical vortices.

Because of their high peak power, short laser pulses are highly beneficial for nonlinear optics. However, most nonlinear vortex experiments to date use relatively long-pulses or cw-lasers. This is because most methods for vortex generation suffer from chromatic aberrations. Nevertheless, depending on the spectral extent of the incident pulses optical vortices can also be imprinted on femtosecond laser beams using spectrally compensating techniques [23, 24, 25], or spiral phase plates [26]. Such generation of dispersion-free high-intensity vortex beams enables studies of nonlinear vortex propagation in a much wider range of (even weakly) nonlinear materials. As such, nonlinear vortex beam filamentation in air [27] and water [28] has been investigated.

An important benefit of using high intensity short pulses is the possibility to observe cascaded nonlinear processes, such as cascaded Raman scattering [29, 30] and nondegenerate four-wave mixing [31, 32, 33]. To date, no cascaded nonlinear four-wave mixing process with singular optical beams as predicted in [29] has been experimentally demonstrated. While the generation of white-light supercontinuum from vortex beams has been attempted in glasses [34], the breakup of the vortex ring into single filaments fully destroyed the spatial coherence of the beam. An important practical issue to address here is a precision control of the nonlinearity strength required to reduce the effect of filamentation and improve the coherent transfer of the

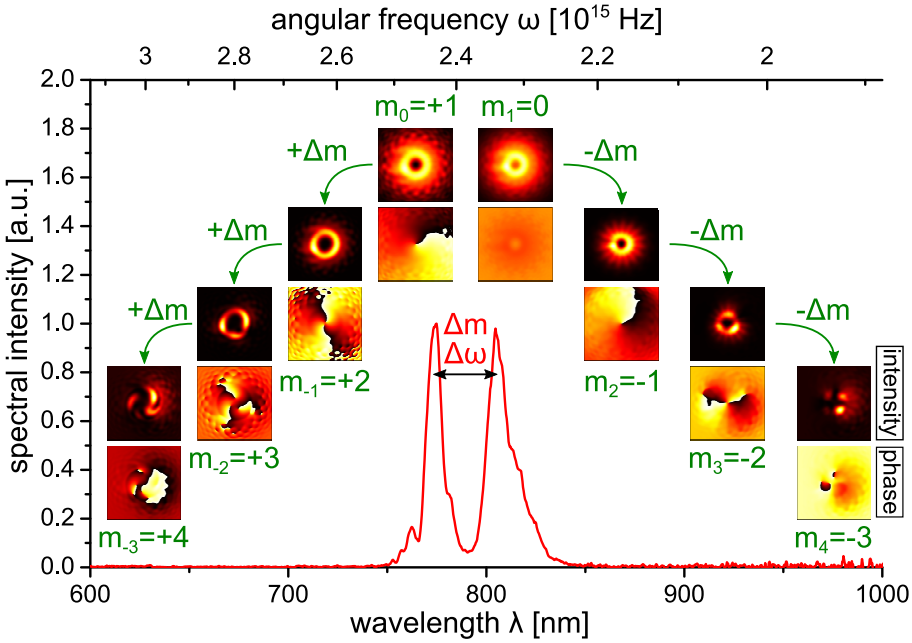

Fig. 1. Algebra of vortex beams with increased topological charge due to cascaded four-wave mixing. The experimental double-peak input spectrum is shown in red, together with simulated intensity (top) and phase (bottom) profiles after nonlinear propagation for the mixing of a Gaussian beam with a vortex of unit TC. The magnitude of the TC changes by 1 with the order of the cascading process, which can be seen in the steeper phase spirals further away from the pump beams. The intensity profile in 3rd order already shows distortion due to strong intensity dependence.

phase throughout the nonlinear cascade.

2. Vortex four-wave mixing

Here we demonstrate the generation of broad spectrum singular beams through cascaded four-wave mixing (FWM). By careful intensity control and the use of dual frequency pump pulses we are able to identify the process of cascaded FWM and reduce the (multi-)filamentation of the vortex beam. Experiments performed with vortex beams of different TC show cascaded nonlinear TC mixing up to 3rd order and are in excellent agreement with frequency-domain numerical simulations. Starting with pump pulses of bandwidth of 43nm, vortices can be observed within >200nm after nonlinear propagation. FWM is a third-order nonlinear process, where four optical fields interact in a nonlinear Kerr medium: $\omega_d = \omega_a + \omega_b - \omega_c$. In our case, initially only two distinct pump beams of frequencies $\omega_0 > \omega_1$ are present. Energy conservation dictates the resulting photon energy when combining any three photons of those pump beams, generating spectral satellites $\omega_n = \omega_0 - n\Delta\omega$. This process becomes cascaded if the intensity of the generated side-bands is sufficiently high, leading ultimately to a frequency comb, where side-bands are spaced by the difference frequency $\Delta\omega = \omega_0 - \omega_1$, similarly to what has been observed in ring microcavities, see, e.g. [35]. The TC conversion in the cascaded process has to obey the transformation law analogous to the one for the frequency: $m_n = m_0 - n\Delta m$ with $\Delta m = m_0 - m_1$ [29, 31]. Labelling the pump beams ω_0 ="blue" and ω_1 ="red" (for obvious reasons) with TCs m_0, m_1, the TC of the spectral satellites $n = -1, \pm 2, \pm 3, \ldots$ can thus be cal-

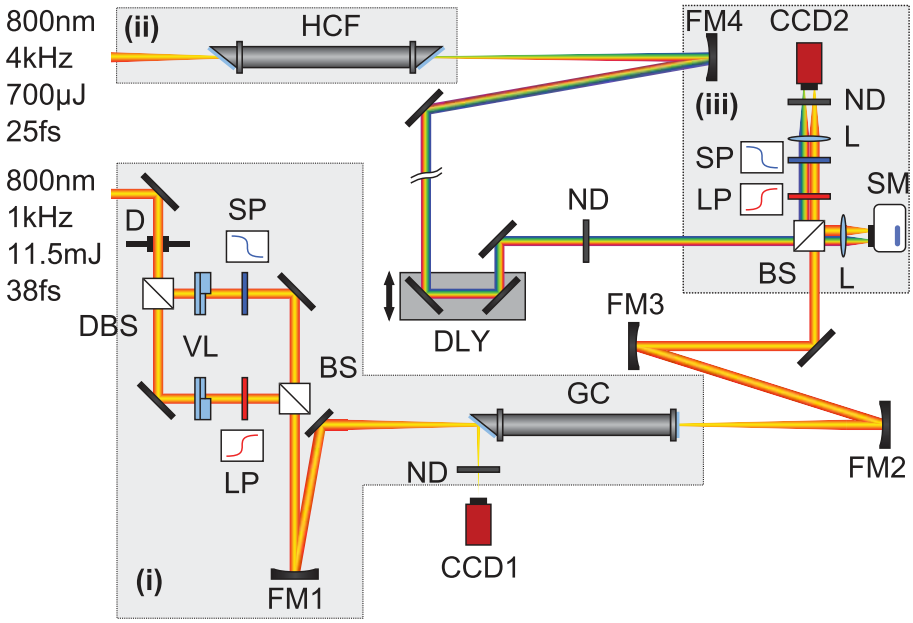

Fig. 2. Experimental setup. i) Vortex generation and FWM, ii) reference beam generation, iii) output characterization. D: Iris, DBS: dichroic beamsplitter, VL: vortex lens, SP: short-pass filter, LP: long-pass filter, BS: beamsplitter, FM1: focusing mirror f=2m, GC: gas cell, FM2: collimating mirror f=3m, FM3: collimating mirror f=4m, ND: ND filter, CCD: CCD-camera, SM: spectrometer, HCF: hollow-core fiber (filled with Ne gas), FM4: collimating mirror f=1m, DLY: delay stage.

culated. Each spectral satellite carries a defined TC, which represents an arithmetic progression of the topological charge in the spectral satellites, as shown in Fig. 1.

3. Experimental setup

In order to generate pump beams with sufficient spectral separation, an 11.5mJ, 38fs, 1kHz Ti:Sapphire amplified pulse is split with a dichroic beam splitter (cut-on wavelength 800nm) (see Fig. 2). The resulting spectral peaks are centered at 775nm (”blue”) and 805nm (”red”). A helical phase with TC $m = \pm 1$ can be imprinted on either or both beams with 16-step, AR-coated spiral phase plates (also called vortex lenses / VLs). After additional spectral filtering and recombination with a low-dispersion broadband beamsplitter, the remaining average power is 2.0W, with approximately equal intensity in both beams.

The vortex beams are then focused with a f=2m spherical mirror (FM1 in Fig. 2) into a gas cell. The Fresnel reflection from the entrance window is used to ensure spatial overlap of the pump beams in the focus. Temporal overlap is achieved by maximizing the white light emission when the cell is filled with Argon. For the actual measurement, the gas cell is evacuated and nonlinear wave mixing is observed in the 3mm thick fused silica entrance window only. In this way, deteriorating effects especially due to plasma in the focus are avoided, and the peak intensity within the window can be controlled by adjusting the distance between the focusing mirror FM1 and the gas cell. Nonlinear effects in the exit window play a negligible role due to large distance from the focus and smaller window thickness (1mm). The diffraction length of the beam is L_D=4cm, while the nonlinear length L_{NL} (corresponds to a nonlinear phase

shift of 1) can be tuned from few hundreds of microns to several centimetres. By adjusting the ratio L_{NL}/L_D we can control the amount of spectral broadening and delay development of the modulational instability across the beam profile. With the setup adjusted for low fluctuation at the output, the peak intensity inside the entrance window is estimated to be $1.1 \cdot 10^{10}$W/cm^2. This results in a nonlinear phase shift $B = k_0 \int_0^L n_2 I_{peak}(z) dz \approx 0.1$ inside the entrance window glass. After the gas cell, the beam is recollimated and interfered with a reference beam from a gas-filled hollow-core fibre (see Fig. 2). This beam, usually used for few-cycle pulse generation, possesses a near-Gaussian spatial profile and covers the full visible spectral range, thus making it a suitable reference for interferometric spatial phase measurements.

The interference pattern and intensity profiles are observed on another CCD camera in slightly focused geometry. As a signature of the vortex helical phase, the dislocation is visible as a fork-like splitting of the interference stripes. The direction of the splitting (”fork up”/”fork down”) corresponds to the direction of the angular phase slope (clockwise/counter-clockwise), whereas the number of fork rakes indicates the topological charge $m+1$ (for integer values of m).

The images are recorded after spectral edge-pass filters with cut-on wavelengths corresponding to the gaps between the expected central wavelengths of the spectral satellites. This method is justified because the generation efficiency is expected to decrease rapidly with the cascading order of the process. This way, only the dominant part of the spectrum close to the filter edge is contributing to the interference pattern. The signal vanishes when either of the two arms in the first interferometer is blocked, as expected for a nonlinear generation mechanism. For the outermost spectral regions, multiple shots (5-10) had to be integrated. This leads to blurring of the interferograms, but the TC can still be determined from the different number of fringes on top and bottom of the vortex ring. Apart from that, the data shown are all single-shot measurements.

4. Experimental results

Fig. 3 shows the obtained phase-dependent interference patterns and intensity profiles for three different fundamental scenarios: The top row [Fig. 3(a)] shows pump beams with equal TC $m_0 = m_1 = +1$, $\Delta m = m_0 - m_1$. This is an important case because all spectral satellites have the same topological charge ($m_n = +1$), which allows the generation of white-light vortex continuum in the multiply cascaded process. Although a single vortex beam of sufficient bandwidth could be used in this case, we keep the two peak spectrum for consistency. Indeed vortices of charge $m_n = +1$ are observed throughout the entire accessible spectral bandwidth of the beam, which is only limited by increasing disintegration of the intensity profile for very remote wavelengths. The respective numbers of the spectral satellites together with their theoretical central wavelengths are denoted in the top row.

The mixing of a vortex with a Gaussian beam is shown in the second row. In this case, the topological charge increases/decreases by one with the order of the satellite peak. Fig. 3(b) shows only the case for a ”red” Gaussian mixed with a ”blue” vortex, because the results are qualitatively similar for the reversed case. Yet interesting to note is the fact that we observe stronger generation of satellites on the spectral side adjacent to the vortex pump. The measured beam profiles for this case are also given in Fig. 3(c). Within the outermost spectral satellites, disintegration of the vortex ring by the modulational instability is observed [28], due to larger sensitivity to shot-to-shot fluctuations. Finally, we examine the case of two counter-rotating vortices of charge $m_0 = +1$ and $m_1 = -1$ [fourth row - Fig. 3(d)]. In this case, since $\Delta m = 2$, we observe the expected increase (decrease) of the vortex charge by 2 with the order of the cascaded process. We are able to record interference patterns up to 3rd order (charge +7) on the blue side, and up to 2nd order (charge -5) on the red side of the spectrum. For this largest TC difference between the two pump beams, we observe the cleanest beam profiles

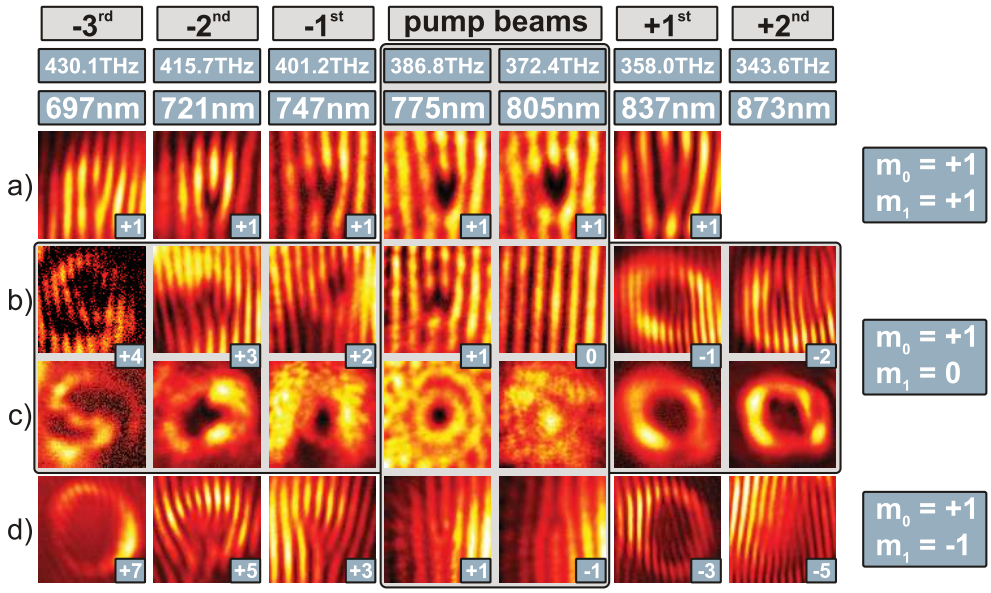

Fig. 3. Experimental interferograms and beam profiles for different vortex pump beams after nonlinear four-wave mixing. The pump beams are highlighted in grey. The respective central frequencies and wavelengths of the spectral satellite/pump beam along with the cascading order of the FWM process are denoted on top. a) Two vortices of equal TC $m_0 = m_1 = +1$, b) Vortex and Gaussian TCs $m_0 = +1$ and $m_1 = 0$, c) corresponding intensity profiles for case b), d) Two vortices of opposite TCs $m_0 = -m_1 = +1$. Contrast has been enhanced slightly for the -3rd order interferograms. The number in each box indicates TCs of the generated vortices.

with very low disintegration of the vortex intensity ring. This effect can partially be attributed to the almost identical divergence of the two pump beams due to the same modulus of the TC. It is known that vortices of TC $|m| > 1$ are unstable against perturbation even in the linear regime. In all cases where we generate higher-order vortex charge states $|m| > 1$, we observe decay into singly-charged vortices. This decay is a general feature of vortices generated from nonlinear processes, where the nonlinearity acts as a perturbation of the background beam. In self-focusing Kerr media as well as attractive BECs this leads to break-up of the vortex ring into spiralling filaments, which finally can collapse [36, 37]. In most cases however, the fundamental vortices remain closely together, so that a dark core can be observed. Since the relatively stable vortices are observed in our experiment and the frequency spectrum is equidistant, we can conjecture that the spatiotemporal spiralling predicted in [29] is a likely to be present, but not yet characterized, feature of our observations.

5. Numerical Simulations

The theoretical model describing the interaction between the different vortex beams is a set of 10 coupled nonlinear Schroedinger-type equations in the spectral domain. The slowly-varying amplitudes A_n with respective wavenumbers k_n follow the equations

$$i\frac{\partial A_n}{\partial z} + L_D^0 k_n A_n + \frac{k_0}{2k_n}\Delta_\perp A_n + \gamma(|A_n|^2 A_n + 2\sum_{n\neq m}|A_m|^2 A_n + H_n) = 0. \qquad (1)$$

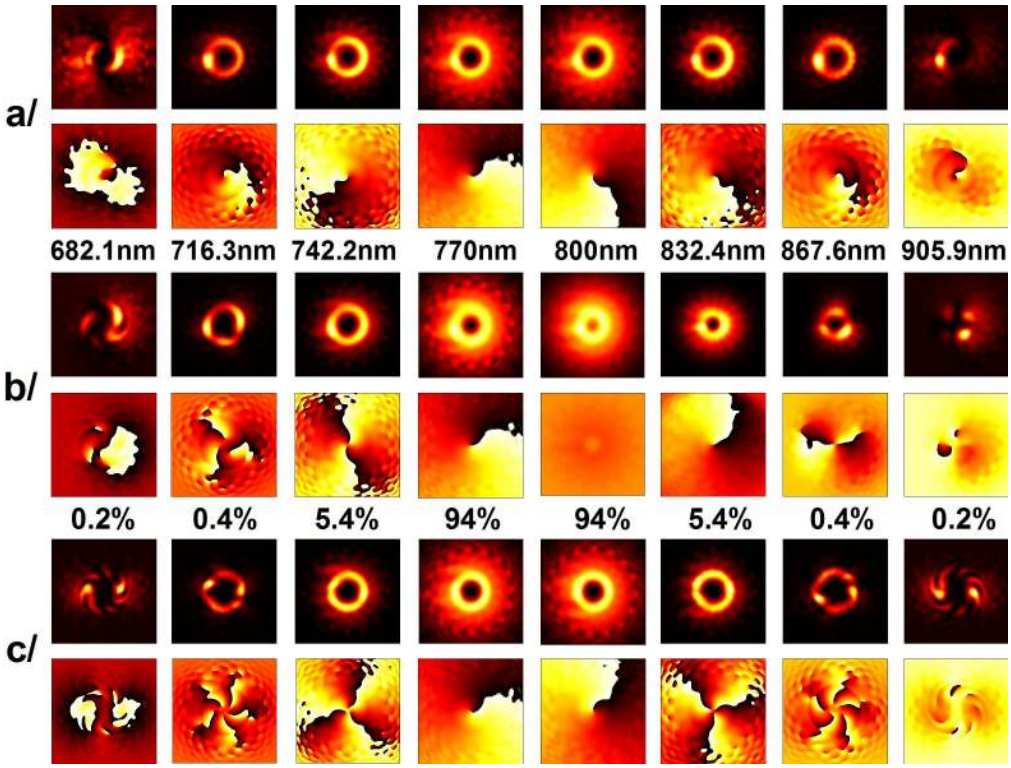

Fig. 4. tanh-vortices: Intensity (odd rows) and phase (even rows) of the pump waves at 770nm and 800nm and of 6 of the newly generated waves in the observation plane (one diffraction length L_D^0 away from the exit of the nonlinear medium of length L_D^0). The outermost spectral components are left out due to already too strong diffraction. Case a/ - pump vortices with identical charges; Case b/ - pump vortex and Gaussian beams; Case c/ - pump vortices of opposite charges. Separators - central wavelengths of the simulated waves and estimated conversion efficiencies. Some 16% of the total computational window is shown in each frame. See text for further details.

The model accounts for linear dispersion and diffraction, as well as nonlinear self- and cross-phase modulation, four-wave mixing and saturation of the nonlinearity via $\gamma = \gamma_0/(1+I/I_{sat})$. For reasons of simplicity, we show here the terms H_n and corresponding phase mismatches Δk_i for a 4 wave model only (2 pump beams $n = 0, +1$ and 2 signal beams $n = -1, +2$):

$$\begin{aligned}
H_{+2} &= 2A^*_{-1}A_0A_{+1}exp(i\Delta k_1 zL_D^0) + A_0^*A_{+1}^2 exp(i\Delta k_2 zL_D^0),\\
H_{+1} &= 2A_{-1}A_0^*A_{+2}exp(i\Delta - k_1 zL_D^0) + 2A_0A_{+1}^*A_{+2}exp(-i\Delta k_2 zL_D^0)\\
&\quad + A^*_{-1}A_0^2 exp(i\Delta k_3 zL_D^0),\\
H_0 &= 2A_{-1}A^*_{+1}A_{+2}exp(i\Delta - k_1 zL_D^0) + 2A_{-1}A_0^*A_{+1}exp(-i\Delta k_3 zL_D^0)\\
&\quad + A_{+1}^2A^*_{+2}exp(i\Delta k_2 zL_D^0),\\
H_{-1} &= 2A_0A_{+1}A^*_{+2}exp(i\Delta k_1 zL_D^0) + A_0^2A^*_{+1}exp(i\Delta k_3 zL_D^0),
\end{aligned} \tag{2}$$

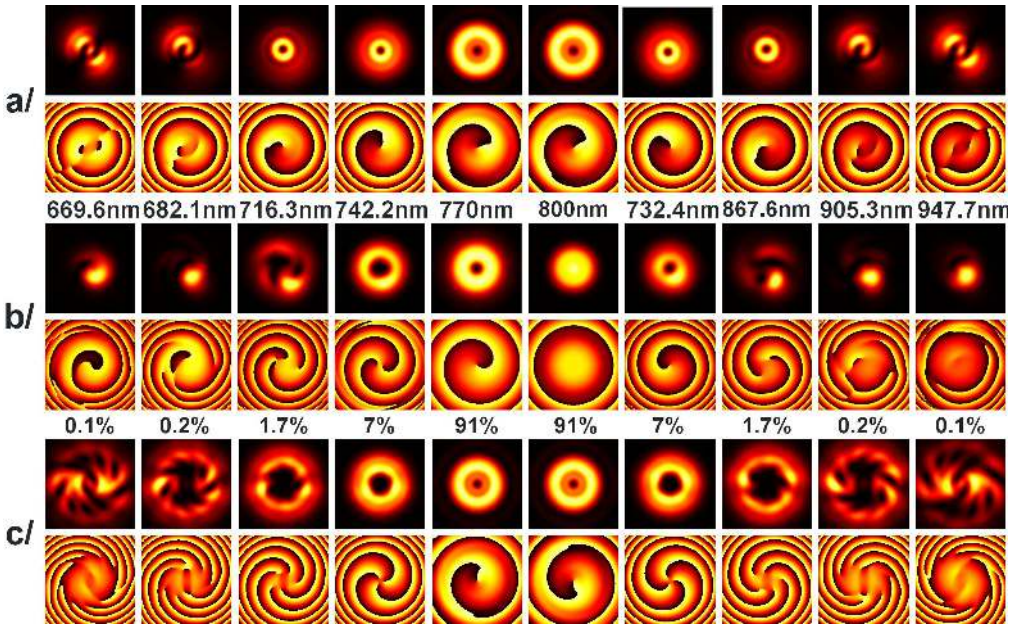

Fig. 5. r-vortices: Intensity (odd rows) and phase (even rows) of the pump waves at 770nm and 800nm and of the newly generated waves in the observation plane (one diffraction length L_D^0 away from the exit of the nonlinear medium of length $0.5L_D^0$). Case a/ - pump vortices with identical charges; Case b/ - pump vortex and Gaussian beams; Case c/ - pump vortices of opposite charges. Separators - central wavelengths of the simulated waves and estimated conversion efficiencies. Some 16% of the total computational window is shown in each frame. See text for further details.

$$\begin{aligned}\Delta k_1 &= k_0 - k_{-1} + k_{+1} - k_{+2},\\ \Delta k_2 &= 2k_{+1} - k_0 - k_{+2},\\ \Delta k_3 &= 2k_0 - k_{-1} - k_{+1}.\end{aligned} \tag{3}$$

The initial values for the simulation were chosen as follows: All spectral components except for the central pump beams ($n = 0, +1$) are set to an effective zero (ten orders of magnitude weaker than the pump components). The pump beams are modeled as either fundamental r-vortices with a continuously varying azimuthal phase

$$A(r,\phi) = A_0 (r/r_0)^{|m|} \exp(-r^2/r_0^2) \exp(im\phi), \tag{4}$$

or as tanh-vortices with a 16-level stepped phase profile, as in the experiment

$$A(r,\phi) = A_0 \exp(-r^2/r_{BG}^2) \tanh(r/r_0) \exp\{i \times m \times (2\pi/16) \times int[16\phi/(2\pi)]\}. \tag{5}$$

.

In the tanh case, the core width r_0 is chosen to reflect the experimentally measured beam profiles and $r_0 < 10 r_{BG}$. The longitudinal coordinate is normalized to the diffraction length $L_D^0 = k_0 r_0^2$ of the OV beam at frequency ω_0, and the intensity in the simulations is kept identical to the one needed to form a one-dimensional dark spatial soliton of the same width r_0 (calculated from inverting the sign of γ). All relevant FWM nonlinear terms H_n in the model

equations 2 were generated by using a program for symbolic computations and were subsequently exported to a program code written in Objective-C, which realized a modification of the split-step Fourier method. The computational grid for each wave spanned over 1024x1024 grid points. The numerical results obtained after $2L_D^0$ free-space propagation from the vortex lens (VL) to the entrance of the nonlinear medium of length $1L_D^0$, followed by one diffraction length free-space propagation to the observation plane, are summarized in Fig. 4. Cases a/ and c/ correspond to pump vortices of equal and opposite topological charges, respectively, whereas case b/ presents the results for vortex and Gaussian pump beams. The pump beams are chosen to have central wavelengths of 770nm and 800nm. All necessary refractive indices (and wave numbers) are calculated according to the revised Sellmeier equations [38] at the indicated pump and signal wavelengths, which are also used as separator in Fig. 4. The second row of numbers in the same figure shows the estimated conversion efficiencies (100% initial signal in each pump wave and 0.1% integration accuracy). For better visibility we present in Fig. 4 only six newly generated spectral components, in which the vortices are clearly formed. Inspecting the phase profiles of the generated spectral satellites one can see that their TCs follow the expected relation $m_n = m_0 - n\Delta m$ with $\Delta m = m_0 - m_1$, where ω_0 corresponds to 770nm, ω_1 to 800nm, and n is the (cascading) order of the process. In Fig. 5 we present results obtained after $1L_D^0$ free space propagation of the pump beams carrying r-vortices from the VL to the entrance of the nonlinear medium (NLM) of length $0.5L_D^0$ followed by $1L_D^0$ free space propagation to the observation plane. Because for r-vortices the widths of the vortex core and the background beam are coupled (see Eq. 4) the length of the NLM was chosen to be shorter in order to keep the slowly-varying envelope approximation of the model equations 2 valid by keeping the pump-induced satellite-beam's focusing reasonably weak. Qualitatively, the results for the FWM TC transfer with r-vortices confirm these for tanh-vortices. We also developed a 28 component model able to more accurately account for the broadband pump. Since it confirms the main predictions of the presented 10-component model, we would like to only mention that its results for the output supercontinuum spectrum fairly well reproduce the measured one when starting the simulations with the measured input pump spectra. These results confirm that the generation of ultra-broad spectrum vortex beams takes place mainly through cascaded four-wave frequency mixing process, whereas spectral broadening due to nonlinear self- and cross-phase modulation remains relatively weak. While our model neglects the full spatiotemporal dynamics of the process and accounts in a simplified way for the influence of the generated plasma in the gas cell, in view of the presented experimental data it accurately captures the spectral reshaping and the spatial structure of the newly generated spectral satellites in the output beam.

6. Discussion and Conclusions

The presented results agree well with the performed frequency-domain numerical simulations. In contrast to the numerical simulations, the experiment is done with pump beams of finite bandwidth, which gives rise to competing four-wave mixing between frequencies of the *same* pump pulse. This effect increases the bandwidth of the pump pulses (and satellites of sufficient intensity), yet it only generates TC *already present* in the respective spectral peak. The basic interaction scenario between adjacent spectral peaks is therefore unaffected, as long as spectral overlap (interference) remains small. To account for the finite bandwidth of the pump pulses, the numerical simulation is extended to use more than one frequency per pump beam. This quasi-pulse regime however qualitatively preserves all features predicted in the dual-frequency pump model.

The presented method is applicable if the acquired nonlinear phase remains reasonably low, so that self-focusing of beam inhomogenities remains limited. Since nonlinear interaction is stronger in the most intense parts of the beam, a homogenous background beam (super-

Gaussian or flat-top) appears to be desirable here. Obviously a trade-off between achieved bandwidth and vortex-ring integrity has to be made due to modulational instability [28]. An approach to limiting deteriorating effects appears to be the use of saturable nonlinear media, e.g. via competing higher-order nonlinearities, which would make the process more controllable [39].

In conclusion, we have demonstrated broadband cascaded mixing of vortex beams in a self-focusing Kerr medium. The nonlinear generation process, although not phasematched, is efficient enough to allow for observation of vortices over a bandwidth larger than 200nm. This constitutes the first measurement of topological charge for a multiply cascaded four-wave mixing process with vortex beams. Topological charge conservation for the nonlinear wave mixing process is found to be fulfilled, and decay of higher-order vortices into fundamental vortices has been observed due to instability arising from the nonlinear self-focusing. The presented results constitute basic scenarios for the interaction between fundamental topological modes, which can be seen as basic "building blocks" to generate complex coherent broadband wave fields with a defined phase structure, which could be used e.g. as elaborate pump/probe beams in coherent control applications or excitation and manipulation of BECs. In the case of identical pump beams (which can be seen as a special case of a single broadband vortex pump beam), the four-wave mixing even preserves the TC, thus rendering the method suitable for the generation of supercontinuum white light vortex beams. Unlike Raman scattering, FWM can be employed in a collinear geometry, eliminating the need for additional angular dispersion compensation.

7. Acknowledgements

A.D. thanks the Institute of Optics and Quantum Electronics, FSU-Jena, Germany, for the warm hospitality during his research stay. This work was partially supported by the National Science Foundation (NSF)-Bulgaria and the Australian Research Council. P.H. acknowledges funding by the DFG. D.N.N. thanks A. Desyatnikov and Y.S. Kivshar for useful discussions.